
This manuscript is prepared for *The Journal of Physical Chemistry C*. Please note that, the manuscript is a non-peer reviewed preprint submitted to EarthArXiv. The final printed version of this manuscript may have slightly different content and will be available via the 'Peer-reviewed Publication DOI' link. Please feel free to contact the corresponding author. Any feedback will be greatly appreciated.

1 **Energetics of Interfacial Interactions of Hydrocarbon Fluids with Kerogen and**
2 **Calcite using Molecular Modeling**

3

4 Zelong Zhang,^{*,†} Haoran Liu,^{‡,⊥} and Jianwei Wang^{†,§}

5

6 [†]Department of Geology and Geophysics, Louisiana State University, Baton Rouge, LA
7 70803, United States

8 [‡]Department of Experimental Statistics, Louisiana State University, Baton Rouge, LA
9 70803, United States

10 [⊥]Department of Oceanography and Coastal Sciences, Louisiana State University, Baton
11 Rouge, LA 70803, United States

12 [§]Center for Computation and Technology, Louisiana State University, Baton Rouge, LA
13 70803, United States

14 Corresponding to: zelongz@lsu.edu

15

16 **Abstract**

17 The fluid-rock interactions are essential to characterize the behavior of petroleum fluids
18 in reservoir formations. Such understanding is difficult to obtain due to the heterogeneous nature
19 of hydrocarbon systems. This study investigated the interactions of light oil molecules with
20 kerogen and calcite using Molecular Dynamics simulations. Specifically, octane and octanthiol
21 were used as model molecules for non-polar and polar oil compounds; a kerogen fragment
22 molecule was employed as the building block for kerogen, the major constituent of reservoir
23 rock organics; calcite as a model system for hydrophilic materials in reservoir rocks. Umbrella
24 Sampling method combined with the Weighted Histogram Analysis Method was deployed to
25 calculate the free energy profiles of oil molecule desorption from kerogen and calcite surfaces.
26 The effects of oil molecular polarity, size of oil molecular cluster, and the presence of water on
27 the interfacial interactions were evaluated based on the free energy profile of desorption. The
28 results show the free energy of desorption of oil molecules significantly decreases at both
29 kerogen and calcite surfaces if water is presented. For the polar oil molecule, the free energy of
30 desorption is higher than that of non-polar oil at both calcite and kerogen surfaces. The kerogen
31 surface exhibits stronger binding energies of oil molecules than the calcite. These findings
32 suggest that 1) polar oil compounds require more effort to be recovered than non-polar ones from
33 the reservoir rocks, 2) isolated oil molecules or oil clusters of a smaller size are harder to be
34 displaced from the surfaces than a larger size of molecular clusters, and 3) the presence of water
35 decreases the free energy of desorption at both surfaces. The results provide an energetic
36 perspective of the interfacial interactions for the oil recovery in reservoir formations. This study
37 demonstrates that the capability of MD simulation in evaluating the impact of different factors on
38 the interfacial interactions for the fundamental understanding of the oil recovery processes in
39 petroleum reservoirs, which can provide valuable implications for developing novel technologies
40 of oil recovery.

41 INTRODUCTION

42 Oil is the main energy source for our modern civilization and will remain as a major
43 contributor of global energy in the foreseeable future.¹ However, only a portion of oil preserved
44 in a reservoir can be recovered. Thus, it is imperative to improve the recovery efficiency of
45 petroleum reservoirs. Current methods to improve oil production including primary, secondary,
46 and tertiary oil recovery techniques can yield 30 to 60 % of the original oil in place, leaving up to
47 70% of the original oil in a reservoir.^{1,2}

48 The pressing demand of energy from modern civilization has spurred technical
49 innovations to improve oil recovery, especially through tertiary oil recovery or enhanced oil
50 recovery. However, there is a limited understanding of how hydrocarbon-bearing fluids interact
51 with the materials in reservoir formations. This knowledge gap impairs the assessment of the
52 economic potential of a hydrocarbon reservoir. For example, relative permeability, an essential
53 parameter of fluid flow characteristics for formation evaluation, is measured by Special Core
54 Analysis (SCAL) through conducting flow experiments on core plugs taken from a reservoir.
55 However, SCAL results are often contradictory or cannot be properly implemented in the
56 reservoir modelling and petrophysical evaluation.³⁻⁵ A myriad of factors may complicate the
57 results, including the hydrofracture geometries, networks of preexisting fractures, adsorption and
58 desorption processes, non-Darcy multiphase flow, chemically and structurally heterogeneous
59 formations, etc.⁶

60 The interfacial interactions between the fluid and rock play a key role in all these
61 complications. As shown in Figure 1, if a pore has a less than 100 nm radius and the
62 intermolecular interaction has an effective distance of 3 nm, a significant portion (12% – 100%
63 volume) of confined fluid can be directly affected by the interfacial interactions. Therefore, to

64 further improve recovery efficiency, a fundamental understanding of the fluid-rock interactions
65 is indispensable.

66 To probe the interfacial interactions at nanoscales, molecular-level characterization is
67 necessary. Both experimental and computational approaches have been applied to study the
68 hydrocarbon fluid behavior in the rock at nanoscale. Extensive experimental studies have been
69 conducted on the reservoir formations to characterize the organic content^{7,8}, pore structure⁹⁻¹²,
70 and petrophysical properties^{11,13-15}. These studies aimed to calibrate the empirical models in
71 reservoir engineering to describe the fluid flow^{16,17} and to provide a basis for reservoir
72 assessment and production optimization.¹⁸ However, due to the compositional and structural
73 heterogeneity of reservoir formations, it is challenging to interpret the dynamics and kinetics of
74 interface interactions without knowing the molecular scale details. Current understanding of the
75 hydrocarbon systems heavily relies on the characterization technologies to conduct experiments
76 on surfaces and interfaces¹⁹⁻²¹ such as Focus Ion Beam Scanning Electron Microscopy (FIB-
77 SEM),^{15,22,23} Transmission Electron Microscopy (TEM),^{23,24} Atomic Force Microscopy
78 (AFM),^{16,25,26} X-ray Diffraction (XRD),^{27,28} X-ray microtomography (Micro-CT),^{29,30} Nuclear
79 Magnetic Resonance (NMR),^{31,32} etc. Implementing these methodologies to characterize
80 microscopic phenomena becomes challenging at the molecular level. Unlike experiments,
81 computational simulations can study physical phenomena over a range of scales,³³ directly
82 connecting the microscopic details of a system to macroscopic properties of experimental
83 interest.³⁴ Due to the intensive computation, Quantum Mechanics (QM) simulations have strict
84 limits on the size, time, and complexity of the systems.³³⁻³⁵ Molecular simulations, built on
85 classical molecular mechanics (MM) such as Monte Carlo (MC) and Molecular Dynamics (MD),
86 are more appropriate than QM methods to address the issues of size and complexity of the

87 hydrocarbon systems. MC methods are stochastic approach, suitable for system equilibrium,
88 while MD techniques are deterministic, suitable for both equilibrium and transport properties of
89 a given system.^{34,35} Thus, this study used MD to investigate the energetics of fluid-rock
90 interactions. Currently, there are several studies using MD to investigate hydrocarbon fluid
91 interactions with kerogen and minerals, such as 1) the adsorption, diffusion, and permeation of
92 hydrocarbon fluid in shale kerogen and kerogen analogue;³⁶⁻⁴³ 2) slippage, displacement, and
93 adsorption of hydrocarbon flow on quartz, calcite slits, and montmorillonite slits;⁴⁴⁻⁴⁷ 3)
94 detachment of oil cluster from silicate surfaces in surfactant solution.⁴⁸ These studies evaluated
95 the effect of nanopores on the properties of hydrocarbon fluid, such as bulk viscosity, contact
96 angle, and slippage with focuses on the phenomena of the interactions. For instance, Liu et al
97 2012 stated that water can penetrate the oil—water interface and form a surface water layer on a
98 hydrophilic silica surface, enhancing the oil detachment from the hydrophilic surface.⁴⁸
99 However, there is a knowledge gap in the energetic aspect of the interactions, which is
100 essentially underexplored. This lack of the knowledge on the thermodynamics of the interactions
101 limits current understanding of the fundamental mechanism in hydrocarbon fluids interactions
102 with reservoir formations.

103 The present study intends to examine the feasibility of the computational approach to
104 evaluate the free energy profile of oil compounds desorption from the surfaces of reservoir rock
105 materials. Umbrella Sampling, widely used in computational biology and biochemistry⁴⁹, was
106 adopted to compute the free energy profiles of the oil interactions with the rock materials in the
107 desorption. We studied the surfaces of kerogen and calcite to evaluate the effect of four different
108 variables including oil polarity (polar vs non-polar oil), oil cluster size (a single molecule oil vs
109 30 molecules oil cluster), surface hydrophobicity (inorganic calcite mineral vs organic kerogen),

110 and surface water (the presence vs the absence of surface water). Probing the free energy
111 changes in oil-rock interactions can provide insight into the thermodynamics of the surface
112 wettability and hydrocarbon behaviors in reservoir formations.

113 **METHODS**

114 *Molecular models for oil, kerogen, and calcite*

115 Crude oil is a mixture of a wide range of polar and non-polar compounds with varying
116 proportions, composition, and molecular weight. Typically, crude oil contains over 45% non-
117 polar (e.g. alkanes and cycloalkanes) and less than 15% polar species (e.g. N-, S-, O- and metal-
118 containing compounds).^{50,51} Polar components can significantly affect properties of hydrocarbon
119 fluid in reservoir such as viscosity, contact angle, interfacial activity, emulsion, and chemical
120 stability.⁵²⁻⁵⁴ The oil-rock interactions are largely attributed by the polar species,⁵⁵ particularly in
121 organic phases which usually retain more polar components than minerals⁵². Thioalkanes are
122 common sulfur compounds found in crude oils.⁵⁶ Crude oil, especially from shale, can has a high
123 content of light oil (C₁-C₉).^{57,58} Therefore, we selected 1-octanethiol (C₈H₁₈S) with a dipole
124 moment of 2.9 D⁵⁹ and its non-polar counterpart n-octane (C₈H₁₈) as the models for polar and
125 nonpolar oil respectively in our simulations as shown in Figure 2. In addition, to model a small
126 oil drop, we prepared two oil clusters consisted of 30 molecules of octanethiol and octane for
127 polar and non-polar oil droplets respectively as shown in Figure 3(c).

128 Reservoir rocks have complex microstructures and mineralogy and contains various
129 amount of inorganic and organic constituents. Major mineral phases include clays, quartz, and
130 carbonates (calcite and dolomite).⁶⁰ Due to its simple structure and ubiquitous presence in
131 formation rocks, the calcite (104) face was chosen as a mode for hydrophilic surface of reservoir

132 rocks. The calcite (104) is a flat stoichiometric surface. It is one of most common mineral faces
133 occurred in both geological and biological systems and has been well studied both
134 computationally and experimentally.⁶¹ The key organic phase in shale involved in the
135 interactions with hydrocarbon fluid is kerogen.^{52,62,63} Despite the complexity of kerogen in
136 reservoir formations⁶⁴, many studies used graphene to represent kerogen^{36,42,43,65–68}. The
137 differences between graphene and kerogen, such as bonding environment of functional
138 groups^{69,70} and surface morphology⁶⁴, give rise to different chemical and mechanical properties
139 and interfacial interactions. These deviations can lead to inaccurate modeling with respect to
140 experimental measurements^{70,71}. To capture fundamental properties of kerogen, we employed a
141 molecular fragment $C_{22}H_{13}ON$ directly derived from type II kerogen to build kerogen surfaces,³⁷
142 which is the most common kerogen in hydrocarbon-bearing shale formations.⁶⁴ The kerogen
143 molecule has five benzene rings, a secondary amine, and a phenol group, making this kerogen
144 molecule a polar compound. To create kerogen surfaces, 511 kerogen molecules were randomly
145 added into a computational supercell (18,907 atoms in total), quenched from 3000 to 300 K. The
146 surface was then created by inserting a vacuum space between the kerogen and lastly a
147 stabilization and a relaxation of the surface were followed at 300 K using an NVT ensemble.

148 The calcite (104) surface in Figure 3(b) was built with 1620 $CaCO_3$ molecule units with a
149 dimension of approximately $7 \times 7 \times 2$ nm with 8,100 atoms. The kerogen surface in Figure 3(a)
150 was built with 511 $C_{22}H_{13}ON$ molecule units with a dimension of approximately $8 \times 8 \times 3$ nm
151 and 18,907 atoms as shown. Because of the ubiquitous presence of water in the reservoir
152 formations, water molecules were added to the fluid. To ensure the oil molecules surrounded by
153 water, 7,250 and 10,000 water molecules were added to the calcite surface of single oil molecule

154 or oil cluster, respectively, while 7,500 and 10,000 water molecules were placed on kerogen
155 surfaces of single oil molecule or oil cluster, respectively.

156 A previous experimental study indicates the calcite (104) surface exhibits neutral charge
157 due to the stoichiometry and alternating of Ca^{2+} and CO_3^{2-} .^{72,73} Kerogen surfaces can be
158 negatively charged due to the deprotonation of functional groups, such as OH and NH. However,
159 classical MD models only simulate interatomic interactions by empirical potentials for bond
160 length, angle, and dihedral, whereas formation and breaking of covalent bonds are not considered
161 unless specified by force field. Both calcite and kerogen surfaces maintain electrical neutrality
162 owing to the charge balance of each model molecule. Layers of alternating Ca^{2+} and CO_3^{2-} on the
163 calcite (104) create a flat surface, while the benzene rings and polar functional groups of kerogen
164 molecule yield highly heterogenous surfaces of kerogen.

165

166 ***Molecular Dynamics (MD) Simulation and Gibbs Free Energy Profiles***

167 MD simulations in this study were deployed using software package GRONingen
168 MACHine for Chemical Simulations (GROMACS).⁷⁴ All simulations employed three-
169 dimensional periodic boundary conditions. The OPLS-AA force field was used to describe oil
170 molecules and kerogen.⁷⁵ The SPC potential is used to describe water molecule.⁷⁶ A previously
171 developed force field was used for calcite.⁷⁷ All these potentials have been tested and are capable
172 of producing satisfactory results on bulk and interfacial properties, which are consistent with
173 experimental data.^{78–80} Newton's equations of motion were integrated using the leap-frog scheme
174 with a timestep of 1 fs, fast Smooth Particle-Mesh Ewald (SPME) electrostatics, Verlet cutoff-
175 scheme, and temperature coupling using a Nose-Hoover extended ensemble with a coupling

176 constant of 0.1 ps. Simulations were visualized by Visual Molecular Dynamics (VMD)
177 package.⁸¹

178 The potential of mean force for the oil interactions with different surfaces was computed
179 by Umbrella Sampling and the Weighted Histogram Analysis Method (WHAM).^{82,83} Gromacs
180 package was used to carry out Umbrella Sampling simulations by running separate simulation
181 windows along the reaction coordinate individually. These windows were generated by
182 extracting a series of configurations from a pulling simulation that drew the oil into or away from
183 the surfaces along the designated reaction coordinate.

184 In each simulation window, umbrella potential, a biased harmonic potential, was applied
185 to the system. For each individual simulation window, a constraint potential with a force constant
186 $9000 \text{ kJ}\cdot\text{mol}^{-1}\cdot\text{nm}^{-1}$ for 0.1 ns to equilibrate the system was first applied, then an umbrella
187 potential with a force constant $9000 \text{ kJ}\cdot\text{mol}^{-1}\cdot\text{nm}^{-2}$ was deployed for 0.1 ns up to 0.2 ns to obtain
188 probability distribution of the given reaction coordinate. With enough sampling overlaps
189 between simulation windows in the entire reaction coordinate space, a free energy profile curve
190 can be calculated by combining data from each window using WHAM.^{82,84}

191 An analysis routine to estimate the errors of the energy profiles was developed using
192 LOESS algorithm in RStudio.^{85,86} This method took the energy profile and employed the
193 bootstrap technique to calculate the confidential intervals at 95% confidence level. The
194 computed errors are listed as shown in Table 1 denoted by brackets. The fluctuation of free
195 energy profile, as shown in Figure S1, is consistent with the size of the estimated error bar.

196

197 **RESULTS AND DISCUSSION**

198 Free energy surfaces in Figures 4-7 show how the system energy changes as a function of
199 the distance between oil compounds and surfaces with respect to their centers of mass. When the
200 oils molecules are close to the surfaces, the energy increases due to repulsive interactions. When
201 the oils gradually move away from the surface, the energy first reaches the minimal point, at
202 which the adsorption occurs at the surfaces. An absence of the minimum suggests zero
203 desorption energy. As the distance continuously increases, the energy increase until the system
204 reaches the energy plateau where no additional energy is required to desorb the oil molecules
205 from the surfaces.

206

207 *Interactions of oil molecules with kerogen surface*

208 The free energy profiles in Figure 4 and Table 1 show the energy changes as a function of
209 the distance between oil compounds and kerogen surface in the presence of water. The
210 desorption energies are 17.0 ± 2.0 kJ/mol and 16.5 ± 3.3 kJ/mol for non-polar and polar single
211 oil molecule and 371 ± 12.4 kJ/mol and 209 ± 7.0 kJ/mol for non-polar and polar oil clusters,
212 respectively. In the absence of water, it is challenging to maintain oil molecules as a cluster at or
213 above 300 K. To stabilize the oil cluster, a series of Umbrella Sampling simulations were carried
214 out under lower system temperatures to extrapolate the desorption energy to 300 K (detail was
215 discussed in Figure S3). The desorption energies of the oil clusters on kerogen surfaces are $437 \pm$
216 13.5 kJ/mol for both polar and non-polar (Figure S3). For the single oil molecule, the desorption
217 energies on kerogen in Figure 5 and Table 1 are 23.3 ± 3.5 kJ/mol and 39.5 ± 9.5 kJ/mol for non-
218 polar and polar, respectively.

219

220 *Interactions of oil molecules with calcite (104) surface*

221 The free energy profiles in Figure 6 shows how free energy changes as a function of the
222 distance between oil compounds and the calcite (104) surface in water. Unlike the rest free
223 energy profiles (described later), they exhibit a distinct pattern: as the distance increase, the free
224 energy quickly decreased and then stayed at the same value as the molecule is further away from
225 the surface. Such patterns indicate near zero energy of the desorption of oil molecules on the
226 calcite surface in the presence of water.

227 For comparison, the same systems without water were simulated, of which the free
228 energy profiles are depicted in Figure 7. The results show that 33.6 ± 3.9 kJ/mol and 18.0 ± 5.5
229 kJ/mol are required to desorb polar and non-polar oil molecules from the calcite surfaces
230 respectively, and 222 ± 36 kJ/mol and 198 ± 42 kJ/mol to desorb polar and non-polar oil clusters,
231 respectively. A detailed analysis of the trajectory (Figure S4) suggests that the polar molecule
232 was bound to the calcite surface through the thiol functional group –SH, which confirms a
233 previous study on the adsorption of simple organic molecules on calcite (104).⁸⁷ In addition, the
234 thiol group –SH of polar oil appears to favor the sites of Ca^{2+} site of calcite (104) surface,
235 whereas the non-polar oil shows no preference of absorption sites.

236

237 *Effect of surface composition on the desorption energy*

238 Our study shows that, in general, oil molecules have stronger interactions with kerogen
239 than with calcite regardless of surface environment and oil molecular polarity. Kerogen is an
240 organic compound and usually oleophilic, whose surface property depends on the specific
241 functional groups. The kerogen model in this study contains functional groups such as hydroxyl

242 (–OH) and thiol (sulfhydryl, –SH) groups which inherently exhibit a strong affinity with
243 hydrophilic surfaces while the rest strongly interact with hydrophobic surfaces. On the other
244 hand, calcite, especially the (104) face, is strongly hydrophilic with ionic species Ca^{2+} and CO_3^{2-}
245 on the surface. Therefore, water can be more easily desorbed from the kerogen surface than from
246 the calcite surface, leading to higher desorption energy for oil molecules at the kerogen surface
247 and weak desorption at the calcite surface. Another factor that contributes to the difference
248 between kerogen and calcite is the surface area: calcite has a low surface area which weakens its
249 sorption capacities,⁸⁸ whereas kerogen is porous and waxy according to experimental
250 observations.^{64,89} Thus, the effective surface area on kerogen would be much higher than calcite,
251 leading to a higher desorption capacities for oil.

252 As a result of their different surface properties, the desorption energy at kerogen surface
253 is higher than at the calcite surface: 5.3 to 17 kJ/mol higher for a single oil molecule and 210 to
254 372 kJ/mol higher for the oil cluster (7.0 to 12.4 kJ/mol per molecule for the oil cluster). The
255 difference in the desorption energies of both single molecule oil and oil cluster implies that oil
256 recovery from organic phases of reservoir rock can take more energy than from these highly
257 hydrophilic surfaces of inorganic mineral phases such as calcite.

258

259 *Effect of molecular polarity*

260 Our study shows that the polar oil has a stronger interaction with the kerogen and calcite
261 surfaces than non-polar oil. At kerogen surface, molecular polarity plays an imperative role in
262 the energetics of the oil desorption. These phenomena can be explained by the dipole
263 interactions. Since there is no free ion in the systems, the intermolecular interactions are

264 dominated by permanent dipole interaction, or Keesom interaction. As shown in Figure S5 (a)
265 and (c), the thiol functional group ($-SH$, yellow) of the polar oil tend stay in close proximity to
266 the functional groups of kerogen molecules such as amine ($-NH-$, blue) and hydroxyl ($-OH$, red)
267 upon contact at the interface, which confirms the expected dipole interactions. Unlike the polar
268 oil, non-polar oil molecules have no dipole moment, therefore a weaker desorption energy than
269 the polar oil molecules is expected. Thus, the interactions of the polar oil molecule with kerogen
270 surface is stronger than that of non-polar.⁹⁰ As shown in the Table 1, the desorption energies of
271 the single molecule oil show that the polar oil molecule requires energy about two times of the
272 energy of non-polar per molecule in the absence of water. The desorption energies of single polar
273 and nonpolar oil molecules are approximately the same in the presence of water. For the oil
274 cluster, our calculation indicates that polar oil cluster requires the similar desorption energies as
275 the non-polar oil cluster. These results suggest that the effect of polarity is complicated by
276 kerogen surface property and the presence of water.

277 At the calcite (104) surface, polar oil molecules consistently require higher desorption
278 energies than its counterpart non-polar oil owing to the molecular dipole of the polar oil and the
279 hydrophilic nature of the calcite surface. Although previous studies suggested that calcite (104)
280 is overall non-polar because the alternating Ca^{2+} and CO_3^{2-} are closely packed and charge
281 balance is maintained,^{91,92} the electrostatic interaction between ionic species at the calcite surface
282 and the functional group at the polar molecule favors the adsorption of the polar oil molecules.
283 Therefore, the desorption energy for the polar oil molecule is approximately two times of the
284 desorption energy for the non-polar oil molecule and the desorption energy for the polar oil
285 molecular cluster is approximately 10% higher than the desorption energy for the non-polar oil
286 cluster in the absence of water.

287

288 *Effect of surface water*

289 Our study shows that the presence of surface water reduces the oil desorption energy on
290 all surface conditions, promoting oil desorption in all these cases. As discussed previously, the
291 calcite surface is hydrophilic, while kerogen is both hydrophilic and hydrophobic. The surface
292 water can easily be attracted to the calcite surface and kerogen hydrophilic functional groups.
293 Both water and polar oil molecules have similar dipole moments 2.9 D and 2.27 D,^{59,76}
294 respectively. Water molecules compete with polar oil molecules for adsorption at surfaces with a
295 hydrophilic character, and consequently reducing the desorption energy of the oil molecules at
296 the surfaces. The interactions of waters with the calcite (104) surfaces were much stronger than
297 with kerogen surfaces, suggesting a weaker hydrophilic nature of kerogen surface than the calcite
298 surface. The affinity between calcite and water is stronger than that between calcite and oil,
299 resulting in a strong oil-repellent surface of calcite in the presence of water. As shown in Table
300 1, kerogen surface with water requires much lower energies to desorb oil. For polar oil, the
301 surface water brought a reduction of 50% - 60% on desorption energy to desorb polar oil
302 compound and 15% - 30% reduction for non-polar oil compound. The energy differences
303 between non-polar and polar oil also demonstrate the crucial role of molecular polarity on the
304 fluid-rock interactions. Given the strong hydrophilicity of calcite, the calcite surface becomes
305 oleophobic, jettisoned all the surface oil, in the presence of water. The result provides a
306 fundamental understanding of the role of water in interactions of oil molecules and reservoir
307 materials and in oil recovery.

308

309 *Effect of oil clustering*

310 Our study shows that oil clusters require lower desorption energies per molecule than a
311 single oil molecule. For instance, the desorption energy of a single molecule of polar oil is 4.6 to
312 25.2 kJ/mol higher than the desorption energy per molecule of the oil cluster, which is an
313 increase of 37% to 340% of desorption energy per molecule in the oil cluster. This difference is
314 mainly caused by the number of oil molecules that directly interact with the surface. Not all the
315 molecules in the 30-molecule clusters directly interact with the surfaces, while the single
316 molecule always interacts with the surfaces, which leads to the smaller desorption energies per
317 molecule of a molecular cluster. Although the oil molecular clusters are too small to be
318 comparable with oils in the porous medium in reservoir rocks, the trend quantified in this study
319 suggests that as the pore size decreases, recovering the oil confined in the pores becomes more
320 challenging.

321

322 **CONCLUSIONS**

323 This study demonstrated that Molecular Dynamics simulation is capable of calculating
324 the free energy surface of desorption of single oil molecules and oil molecular clusters at calcite
325 and kerogen surfaces. The results provide fundamental understandings of the interfacial
326 interactions and valuable implications for oil recovery in reservoirs. The main conclusions are as
327 follows.

328 (1) Hydrophobicity of the surface of reservoir materials has a significant effect on the
329 desorption of the oil molecules from the surfaces, leading to a higher free energy cost for

330 oil displacement from organic phases of reservoir rock than from the highly hydrophilic
331 surfaces of inorganic mineral phases such as calcite.

332 (2) The polarity of oil molecules strongly affects the interfacial interactions at both the
333 kerogen and calcite surfaces. The polar oil molecules require more energy to be
334 recovered from both surfaces than non-polar ones. For complex hydrocarbon fluid
335 systems, having a large portion of polar compounds in the oil poses a great challenge. In
336 order to effectively model the interactions between oil and the reservoir materials and to
337 produce reliable results, an accurate description of the polarity of oil molecules is
338 necessary.

339 (3) The presence of water at interface plays a fundamental role in the interactions
340 between oil molecules and reservoir materials. Because of its large dipole moment, water
341 facilitates the oil desorption by interacting with hydrophilic surfaces or sites of either
342 organic kerogen or inorganic minerals.

343 (4) Single oil molecule or small oil molecule cluster dispersed in small nanopores tend to
344 be more challenging to be recovered than large oil molecular clusters due to the stronger
345 interactions of oil molecules with the surfaces.

346 The success of implementing the free energy methods to study the simple hydrocarbon
347 fluid systems paves the way for building more realistic simulations for complex systems by
348 varying temperatures, adding fluid components (e.g. electrolytes, methane, carbon dioxide, and
349 large oil compounds) and introducing other major inorganic phases such as clay minerals and
350 quartz.

351

352 **ASSOCIATED CONTENT**

353 Supporting Information

354 Supporting text 1: Code for error estimation performed by RStudio

355 Supporting text 2: Trajectories of pertinent molecular dynamics simulations

356 Figure S1: Free energy surfaces of oil drop of polar or non-polar oil on calcite surface
357 with water.

358 Figure S2: Free energy surfaces of 30-molecule oil drops interacting with kerogen surface
359 under different temperatures.

360 Figure S3: Desorption energies of 30-molecule oil drops on kerogen surfaces under
361 different temperatures.

362 Figure S4: Snapshot of the simulation trajectory of calcite surface interaction with polar
363 oil molecule in the absence of water.

364 Figure S5: Snapshot of the simulation trajectory of kerogen surface interaction with polar
365 oil molecule in the absence of water at different time step

366 Table S1: Desorption energies of oil drops on kerogen surface under different
367 temperatures in the absence of water.

368

369 **AUTHOR INFORMATION**

370 ORCID

371 Zelong Zhang: 0000-0002-0807-8991

372 Haoran Liu: 0000-0003-0955-3552

373 Jianwei Wang: 0000-0001-7671-0533

374 Notes

375 There are no conflicts to declare.

376

377 **ACKNOWLEDGEMENTS**

378 Z. Z. thanks Dr. Tim J. Tambach (Shell Global Solutions, The Netherlands) and Dr.
379 Erdem Idiz (University of Oxford, UK) for their inspiration to start this project and
380 valuable discussions regarding the scientific challenges in reservoir geochemistry. This
381 research used resources of the National Energy Research Scientific Computing Center
382 (NERSC), a U.S. Department of Energy Office of Science User Facility operated under
383 Contract No. DE-AC02-05CH11231. Portions of this research were conducted with high
384 performance computing resources provided by Louisiana State University
385 (<http://www.hpc.lsu.edu>).

- 387 (1) EIA. *Annual Energy Outlook 2019*; AEO2019; U.S. Energy Information Administration: Washington,
388 DC, 2019.
- 389 (2) Thomas, S. Enhanced Oil Recovery - An Overview. *Oil Gas Sci. Technol. - Rev. IFP* **2008**, *63* (1), 9–19.
390 <https://doi.org/10.2516/ogst:2007060>.
- 391 (3) Forbes, P. The Status of Core Analysis. *J. Pet. Sci. Eng.* **1998**, *19* (1), 1–6.
392 [https://doi.org/10.1016/S0920-4105\(97\)00030-2](https://doi.org/10.1016/S0920-4105(97)00030-2).
- 393 (4) Gao, B.; Kralik, J.; Vo, L.; Shebl, H.; Al Shehhi, R.; Al Jawhari, M. O.; Fullmer, S. State of the Art
394 Special Core Analysis Program Design and Results for a Middle Eastern Carbonate Reservoir;
395 Society of Petroleum Engineers, 2015. <https://doi.org/10.2118/177510-MS>.
- 396 (5) van der Weerd, H.; Masalmeh, S. K.; Jing, X. D.; van Vark, W.; Christiansen, S.; Van Dorp, J. Impact
397 of SCAL (Special Core Analysis) on Carbonate Reservoirs: How Capillary Forces Can Affect Field
398 Performance Predictions. *Petrophysics* **2004**, *45* (05).
- 399 (6) Cueto-Felgueroso, L.; Juanes, R. Forecasting Long-Term Gas Production from Shale. *Proc. Natl.*
400 *Acad. Sci.* **2013**, *110* (49), 19660. <https://doi.org/10.1073/pnas.1319578110>.
- 401 (7) Zhang, T.; Ellis, G. S.; Ruppel, S. C.; Milliken, K.; Yang, R. Effect of Organic-Matter Type and Thermal
402 Maturity on Methane Adsorption in Shale-Gas Systems. *Org. Geochem.* **2012**, *47*, 120–131.
403 <https://doi.org/10.1016/j.orggeochem.2012.03.012>.
- 404 (8) Hutton, A. C.; Kantsler, A. J.; Cook, A. C.; McKirdy, D. M. ORGANIC MATTER IN OIL SHALES. *APPEA J.*
405 **1980**, *20* (1), 44–67. <https://doi.org/10.1071/aj79005>.
- 406 (9) Ross, D. J. K.; Marc Bustin, R. The Importance of Shale Composition and Pore Structure upon Gas
407 Storage Potential of Shale Gas Reservoirs. *Mar. Pet. Geol.* **2009**, *26* (6), 916–927.
408 <https://doi.org/10.1016/j.marpetgeo.2008.06.004>.
- 409 (10) Loucks, R. G.; Reed, R. M.; Ruppel, S. C.; Hammes, U. Spectrum of Pore Types and Networks in
410 Mudrocks and a Descriptive Classification for Matrix-Related Mudrock Pores Spectrum of Pore
411 Types and Networks In Mudrocks. *AAPG Bull.* **2012**, *96* (6), 1071–1098.
412 <https://doi.org/10.1306/08171111061>.
- 413 (11) Sondergeld, C. H.; Ambrose, R. J.; Rai, C. S.; Moncrieff, J. Micro-Structural Studies of Gas Shales;
414 Society of Petroleum Engineers, 2010. <https://doi.org/10.2118/131771-MS>.
- 415 (12) Clarkson, C. R.; Solano, N.; Bustin, R. M.; Bustin, A. M. M.; Chalmers, G. R. L.; He, L.; Melnichenko,
416 Y. B.; Radliński, A. P.; Blach, T. P. Pore Structure Characterization of North American Shale Gas
417 Reservoirs Using USANS/SANS, Gas Adsorption, and Mercury Intrusion. *Fuel* **2013**, *103*, 606–616.
418 <https://doi.org/10.1016/j.fuel.2012.06.119>.
- 419 (13) Passey, Q. R.; Bohacs, K.; Esch, W. L.; Klimentidis, R.; Sinha, S. From Oil-Prone Source Rock to Gas-
420 Producing Shale Reservoir - Geologic and Petrophysical Characterization of Unconventional Shale
421 Gas Reservoirs; Society of Petroleum Engineers, 2010. <https://doi.org/10.2118/131350-MS>.
- 422 (14) Vernik, L.; Milovac, J. Rock Physics of Organic Shales. *Lead. Edge* **2011**, *30* (3), 318–323.
423 <https://doi.org/10.1190/1.3567263>.
- 424 (15) Milliken, K. L.; Rudnicki, M.; Awwiller, D. N.; Zhang, T. Organic Matter-Hosted Pore System,
425 Marcellus Formation (Devonian), Pennsylvania Geohorizon. *AAPG Bull.* **2013**, *97* (2), 177–200.
426 <https://doi.org/10.1306/07231212048>.
- 427 (16) Shabro, V.; Torres-Verdin, C.; Javadpour, F. Numerical Simulation of Shale-Gas Production: From
428 Pore-Scale Modeling of Slip-Flow, Knudsen Diffusion, and Langmuir Desorption to Reservoir
429 Modeling of Compressible Fluid; Society of Petroleum Engineers, 2011.
430 <https://doi.org/10.2118/144355-MS>.

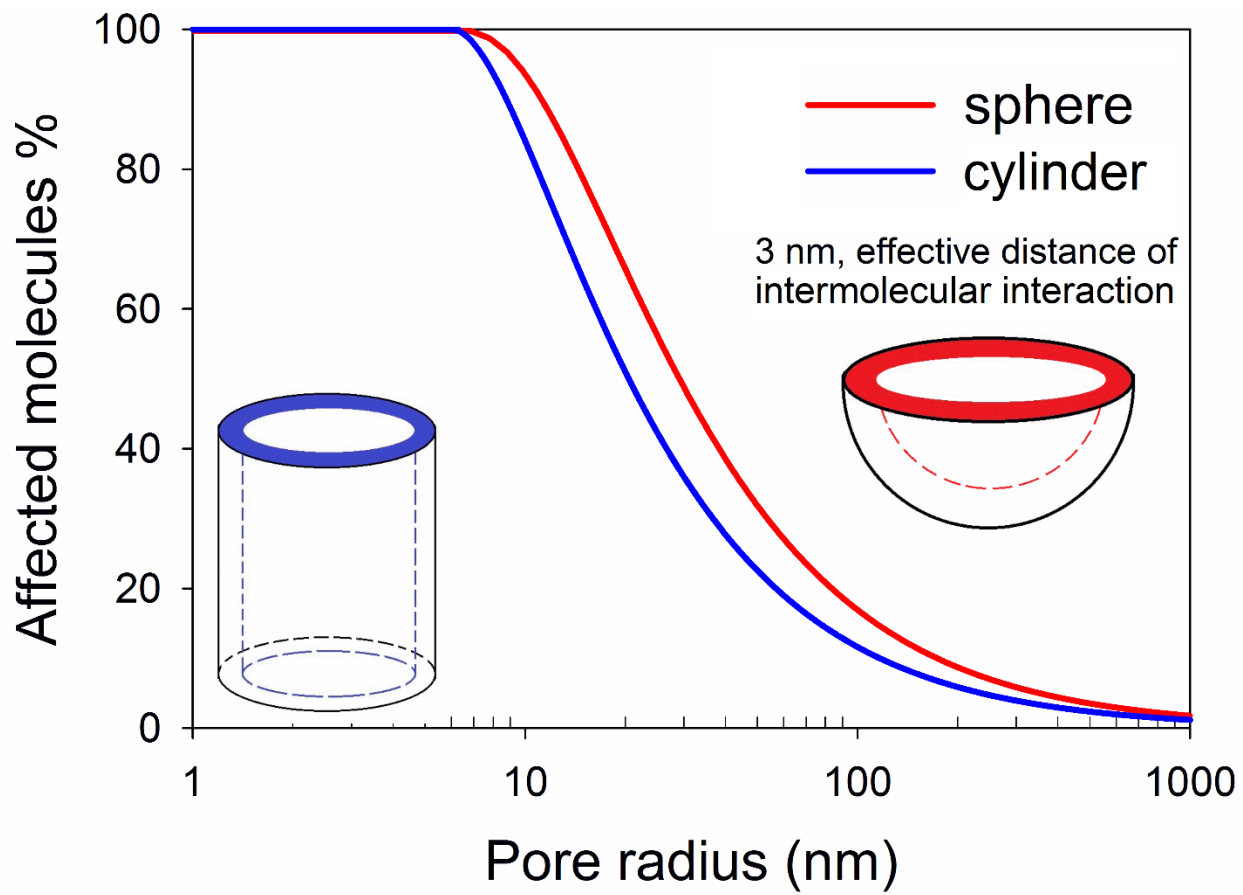
- 431 (17) Wu, K.; Li, X.; Wang, C.; Yu, W.; Chen, Z. Model for Surface Diffusion of Adsorbed Gas in Nanopores
432 of Shale Gas Reservoirs. *Ind. Eng. Chem. Res.* **2015**, *54* (12), 3225–3236.
433 <https://doi.org/10.1021/ie504030v>.
- 434 (18) Wang, F. P.; Reed, R. M. Pore Networks and Fluid Flow in Gas Shales; Society of Petroleum
435 Engineers, 2009. <https://doi.org/10.2118/124253-MS>.
- 436 (19) Zaera, F. Probing Liquid/Solid Interfaces at the Molecular Level. *Chem. Rev.* **2012**, *112* (5), 2920–
437 2986. <https://doi.org/10.1021/cr2002068>.
- 438 (20) *Surface Analysis Methods in Materials Science*; O'Connor, J., Sexton, B., Smart, R., Eds.; Springer
439 Series in Surface Sciences; Springer-Verlag: Berlin Heidelberg, 1992.
- 440 (21) Mineralogical Society of America - Mineral-Water Interface Geochemistry
441 <http://www.minsocam.org/msa/rim/rim23.html> (accessed Mar 13, 2019).
- 442 (22) Milner, M.; McLin, R.; Petriello, J. Imaging Texture and Porosity in Mudstones and Shales:
443 Comparison of Secondary and Ion-Milled Backscatter SEM Methods; Society of Petroleum
444 Engineers, 2010. <https://doi.org/10.2118/138975-MS>.
- 445 (23) Curtis, M. E.; Ambrose, R. J.; Sondergeld, C. H.; Rai, C. S. Transmission and Scanning Electron
446 Microscopy Investigation of Pore Connectivity of Gas Shales on the Nanoscale; Society of
447 Petroleum Engineers, 2011. <https://doi.org/10.2118/144391-MS>.
- 448 (24) Bernard, S.; Horsfield, B.; Schulz, H.-M.; Wirth, R.; Schreiber, A.; Sherwood, N. Geochemical
449 Evolution of Organic-Rich Shales with Increasing Maturity: A STXM and TEM Study of the Posidonia
450 Shale (Lower Toarcian, Northern Germany). *Mar. Pet. Geol.* **2012**, *31* (1), 70–89.
451 <https://doi.org/10.1016/j.marpetgeo.2011.05.010>.
- 452 (25) Javadpour, F. Nanopores and Apparent Permeability of Gas Flow in Mudrocks (Shales and
453 Siltstone). *J. Can. Pet. Technol.* **2009**, *48* (08), 16–21. <https://doi.org/10.2118/09-08-16-DA>.
- 454 (26) Javadpour, F.; Moravvej Farshi, M.; Amrein, M. Atomic-Force Microscopy: A New Tool for Gas-
455 Shale Characterization. *J. Can. Pet. Technol.* **2012**, *51* (04), 236–243.
456 <https://doi.org/10.2118/161015-PA>.
- 457 (27) Bhargava, S.; Awaja, F.; Subasinghe, N. D. Characterisation of Some Australian Oil Shale Using
458 Thermal, X-Ray and IR Techniques. *Fuel* **2005**, *84* (6), 707–715.
459 <https://doi.org/10.1016/j.fuel.2004.11.013>.
- 460 (28) Elgmati, M. M.; Zhang, H.; Bai, B.; Flori, R. E.; Qu, Q. Submicron-Pore Characterization of Shale Gas
461 Plays; Society of Petroleum Engineers, 2011. <https://doi.org/10.2118/144050-MS>.
- 462 (29) Tiwari, P.; Deo, M.; Lin, C. L.; Miller, J. D. Characterization of Oil Shale Pore Structure before and
463 after Pyrolysis by Using X-Ray Micro CT. *Fuel* **2013**, *107*, 547–554.
464 <https://doi.org/10.1016/j.fuel.2013.01.006>.
- 465 (30) Dului, O. G. Computer Axial Tomography in Geosciences: An Overview. *Earth-Sci. Rev.* **1999**, *48* (4),
466 265–281. [https://doi.org/10.1016/S0012-8252\(99\)00056-2](https://doi.org/10.1016/S0012-8252(99)00056-2).
- 467 (31) Kadayam Viswanathan, R. K.; Cao Minh, C.; Zielinski, L.; Vissapragada, B.; Akkurt, R.; Song, Y.-Q.;
468 Liu, C.; Jones, S.; Blair, E. Characterization of Gas Dynamics in Kerogen Nanopores by NMR; Society
469 of Petroleum Engineers, 2011. <https://doi.org/10.2118/147198-MS>.
- 470 (32) Korb, J.-P.; Nicot, B.; Louis-Joseph, A.; Bubici, S.; Ferrante, G. Dynamics and Wettability of Oil and
471 Water in Oil Shales. *J. Phys. Chem. C* **2014**, *118* (40), 23212–23218.
472 <https://doi.org/10.1021/jp508659e>.
- 473 (33) Cygan, R. T. Molecular Modeling in Mineralogy and Geochemistry. *Rev. Mineral. Geochem.* **2001**,
474 *42* (1), 1–35. <https://doi.org/10.2138/rmg.2001.42.1>.
- 475 (34) Allen, M.; Tildesley, D. *Computer Simulation of Liquids*, Second Edition.; Oxford University Press:
476 Oxford, New York, 2017.
- 477 (35) Frenkel, D.; Smit, B. *Understanding Molecular Simulation: From Algorithms to Applications*, Second
478 Edition.; Academic Press: San Diego, 2002.

- 479 (36) Falk, K.; Coasne, B.; Pellenq, R.; Ulm, F.-J.; Bocquet, L. Subcontinuum Mass Transport of Condensed
480 Hydrocarbons in Nanoporous Media. *Nat. Commun.* **2015**, *6*, 6949.
481 <https://doi.org/10.1038/ncomms7949>.
- 482 (37) Collell, J.; Galliero, G.; Gouth, F.; Montel, F.; Pujol, M.; Ungerer, P.; Yiannourakou, M. Molecular
483 Simulation and Modelisation of Methane/Ethane Mixtures Adsorption onto a Microporous
484 Molecular Model of Kerogen under Typical Reservoir Conditions. *Microporous Mesoporous Mater.*
485 **2014**, *197*, 194–203. <https://doi.org/10.1016/j.micromeso.2014.06.016>.
- 486 (38) Collell, J.; Galliero, G.; Vermorel, R.; Ungerer, P.; Yiannourakou, M.; Montel, F.; Pujol, M. Transport
487 of Multicomponent Hydrocarbon Mixtures in Shale Organic Matter by Molecular Simulations. *J.*
488 *Phys. Chem. C* **2015**, *119* (39), 22587–22595. <https://doi.org/10.1021/acs.jpcc.5b07242>.
- 489 (39) Collell, J.; Ungerer, P.; Galliero, G.; Yiannourakou, M.; Montel, F.; Pujol, M. Molecular Simulation of
490 Bulk Organic Matter in Type II Shales in the Middle of the Oil Formation Window. *Energy Fuels*
491 **2014**, *28* (12), 7457–7466. <https://doi.org/10.1021/ef5021632>.
- 492 (40) Sui, H.; Yao, J. Effect of Surface Chemistry for CH₄/CO₂ Adsorption in Kerogen: A Molecular
493 Simulation Study. *J. Nat. Gas Sci. Eng.* **2016**, *31*, 738–746.
494 <https://doi.org/10.1016/j.jngse.2016.03.097>.
- 495 (41) Yiannourakou, M.; Ungerer, P.; Leblanc, B.; Rozanska, X.; Saxe, P.; Vidal-Gilbert, S.; Gouth, F.;
496 Montel, F. Molecular Simulation of Adsorption in Microporous Materials. *Oil Gas Sci. Technol. –*
497 *Rev. D'IFP Energ. Nouv.* **2013**, *68* (6), 977–994. <https://doi.org/10.2516/ogst/2013134>.
- 498 (42) Lee, T.; Bocquet, L.; Coasne, B. Activated Desorption at Heterogeneous Interfaces and Long-Time
499 Kinetics of Hydrocarbon Recovery from Nanoporous Media. *Nat. Commun.* **2016**, *7*, 11890.
500 <https://doi.org/10.1038/ncomms11890>.
- 501 (43) Ambrose, R. J.; Hartman, R. C.; Diaz-Campos, M.; Akkutlu, I. Y.; Sondergeld, C. H. Shale Gas-in-Place
502 Calculations Part I: New Pore-Scale Considerations. *SPE J.* **2012**, *17* (01), 219–229.
503 <https://doi.org/10.2118/131772-PA>.
- 504 (44) Wang, S.; Javadpour, F.; Feng, Q. Molecular Dynamics Simulations of Oil Transport through
505 Inorganic Nanopores in Shale. *Fuel* **2016**, *171*, 74–86. <https://doi.org/10.1016/j.fuel.2015.12.071>.
- 506 (45) Wang, S.; Feng, Q.; Javadpour, F.; Yang, Y.-B. Breakdown of Fast Mass Transport of Methane
507 through Calcite Nanopores. *J. Phys. Chem. C* **2016**, *120* (26), 14260–14269.
508 <https://doi.org/10.1021/acs.jpcc.6b05511>.
- 509 (46) Zheng, H.; Du, Y.; Xue, Q.; Zhu, L.; Li, X.; Lu, S.; Jin, Y. Surface Effect on Oil Transportation in
510 Nanochannel: A Molecular Dynamics Study. *Nanoscale Res. Lett.* **2017**, *12* (1), 413.
511 <https://doi.org/10.1186/s11671-017-2161-2>.
- 512 (47) Underwood, T.; Erastova, V.; Cubillas, P.; Greenwell, H. C. Molecular Dynamic Simulations of
513 Montmorillonite–Organic Interactions under Varying Salinity: An Insight into Enhanced Oil
514 Recovery. *J. Phys. Chem. C* **2015**, *119* (13), 7282–7294. <https://doi.org/10.1021/acs.jpcc.5b00555>.
- 515 (48) Liu, Q.; Yuan, S.; Yan, H.; Zhao, X. Mechanism of Oil Detachment from a Silica Surface in Aqueous
516 Surfactant Solutions: Molecular Dynamics Simulations. *J. Phys. Chem. B* **2012**, *116* (9), 2867–2875.
517 <https://doi.org/10.1021/jp2118482>.
- 518 (49) Kästner, J. Umbrella Sampling. *Wiley Interdiscip. Rev. Comput. Mol. Sci.* **2011**, *1* (6), 932–942.
519 <https://doi.org/10.1002/wcms.66>.
- 520 (50) Hughey, C. A.; Rodgers, R. P.; Marshall, A. G.; Qian, K.; Robbins, W. K. Identification of Acidic NSO
521 Compounds in Crude Oils of Different Geochemical Origins by Negative Ion Electrospray Fourier
522 Transform Ion Cyclotron Resonance Mass Spectrometry. *Org. Geochem.* **2002**, *33* (7), 743–759.
523 [https://doi.org/10.1016/S0146-6380\(02\)00038-4](https://doi.org/10.1016/S0146-6380(02)00038-4).
- 524 (51) Hyne, N. J. *Nontechnical Guide to Petroleum Geology, Exploration, Drilling, and Production*;
525 PennWell Corporation: Tulsa, Okla., 2012.

- 526 (52) Jarvie, D. M. Shale Resource Systems for Oil and Gas: Part 2—Shale-Oil Resource Systems. **2012**,
527 89–119. <https://doi.org/10.1306/13321447M973489>.
- 528 (53) Buckley, J. S.; Liu, Y.; Monsterleet, S. Mechanisms of Wetting Alteration by Crude Oils. *SPE J.* **1998**,
529 3 (01), 54–61. <https://doi.org/10.2118/37230-PA>.
- 530 (54) Sayyouh, M. H.; Hemeida, A. M.; Al-Blehed, M. S.; Desouky, S. M. Role of Polar Compounds in
531 Crude Oils on Rock Wettability. *J. Pet. Sci. Eng.* **1991**, 6 (3), 225–233.
532 [https://doi.org/10.1016/0920-4105\(91\)90015-F](https://doi.org/10.1016/0920-4105(91)90015-F).
- 533 (55) Speight, J. G. The Chemical and Physical Structure of Petroleum: Effects on Recovery Operations. *J.*
534 *Pet. Sci. Eng.* **1999**, 22 (1), 3–15. [https://doi.org/10.1016/S0920-4105\(98\)00051-5](https://doi.org/10.1016/S0920-4105(98)00051-5).
- 535 (56) Composition, Classification, and Properties of Petroleum. In *Chemistry of Fossil Fuels and Biofuels*;
536 Schobert, H., Ed.; Cambridge Series in Chemical Engineering; Cambridge University Press:
537 Cambridge, 2013; pp 174–191. <https://doi.org/10.1017/CBO9780511844188.012>.
- 538 (57) Mango, F. D. The Light Hydrocarbons in Petroleum: A Critical Review. *Org. Geochem.* **1997**, 26 (7),
539 417–440. [https://doi.org/10.1016/S0146-6380\(97\)00031-4](https://doi.org/10.1016/S0146-6380(97)00031-4).
- 540 (58) Yanik, J.; Yüksel, M.; Sağlam, M.; Olukçu, N.; Bartle, K.; Frere, B. Characterization of the Oil
541 Fractions of Shale Oil Obtained by Pyrolysis and Supercritical Water Extraction. *Fuel* **1995**, 74 (1),
542 46–50. [https://doi.org/10.1016/0016-2361\(94\)P4329-Z](https://doi.org/10.1016/0016-2361(94)P4329-Z).
- 543 (59) Kvashnin, D. G.; Antipina, L. Y.; Sorokin, P. B.; Tenne, R.; Golberg, D. Theoretical Aspects of WS2
544 Nanotube Chemical Unzipping. *Nanoscale* **2014**, 6 (14), 8400–8404.
545 <https://doi.org/10.1039/C4NR00437J>.
- 546 (60) Folk, R. L. *Petrology of Sedimentary Rocks*; Hemphill Publishing Company, 1980.
- 547 (61) Kerisit, S.; Parker, S. C. Free Energy of Adsorption of Water and Metal Ions on the {1014} Calcite
548 Surface. *J. Am. Chem. Soc.* **2004**, 126 (32), 10152–10161. <https://doi.org/10.1021/ja0487776>.
- 549 (62) Curtis, J. B. Fractured Shale-Gas Systems. *AAPG Bull.* **2002**, 86 (11), 1921–1938.
550 <https://doi.org/10.1306/61EEDDBE-173E-11D7-8645000102C1865D>.
- 551 (63) Jarvie, D. M.; Hill, R. J.; Ruble, T. E.; Pollastro, R. M. Unconventional Shale-Gas Systems: The
552 Mississippian Barnett Shale of North-Central Texas as One Model for Thermogenic Shale-Gas
553 Assessment. *AAPG Bull.* **2007**, 91 (4), 475–499. <https://doi.org/10.1306/12190606068>.
- 554 (64) Vandenbroucke, M.; Largeau, C. Kerogen Origin, Evolution and Structure. *Org. Geochem.* **2007**, 38
555 (5), 719–833. <https://doi.org/10.1016/j.orggeochem.2007.01.001>.
- 556 (65) Hu, Y.; Devegowda, D.; Striolo, A.; Phan, A.; Ho, T. A.; Civan, F.; Sigal, R. F. Microscopic Dynamics of
557 Water and Hydrocarbon in Shale-Kerogen Pores of Potentially Mixed Wettability. *SPE J.* **2014**, 20
558 (01), 112–124. <https://doi.org/10.2118/167234-PA>.
- 559 (66) Firouzi, M.; Rupp, E. C.; Liu, C. W.; Wilcox, J. Molecular Simulation and Experimental
560 Characterization of the Nanoporous Structures of Coal and Gas Shale. *Int. J. Coal Geol.* **2014**, 121,
561 123–128. <https://doi.org/10.1016/j.coal.2013.11.003>.
- 562 (67) Falk, K.; Pellenq, R.; Ulm, F. J.; Coasne, B. Effect of Chain Length and Pore Accessibility on Alkane
563 Adsorption in Kerogen. *Energy Fuels* **2015**, 29 (12), 7889–7896.
564 <https://doi.org/10.1021/acs.energyfuels.5b02015>.
- 565 (68) Ambrose, R. J.; Hartman, R. C.; Diaz Campos, M.; Akkutlu, I. Y.; Sondergeld, C. New Pore-Scale
566 Considerations for Shale Gas in Place Calculations; Society of Petroleum Engineers, 2010.
567 <https://doi.org/10.2118/131772-MS>.
- 568 (69) Orendt, A. M.; Pimienta, I. S. O.; Badu, S. R.; Solum, M. S.; Pugmire, R. J.; Facelli, J. C.; Locke, D. R.;
569 Chapman, K. W.; Chupas, P. J.; Winans, R. E. Three-Dimensional Structure of the Siskin Green River
570 Oil Shale Kerogen Model: A Comparison between Calculated and Observed Properties. *Energy*
571 *Fuels* **2013**, 27 (2), 702–710. <https://doi.org/10.1021/ef3017046>.

- 572 (70) Bousige, C.; Ghimbeu, C. M.; Vix-Guterl, C.; Pomerantz, A. E.; Suleimenova, A.; Vaughan, G.;
573 Garbarino, G.; Feygenson, M.; Wildgruber, C.; Ulm, F.-J.; et al. Realistic Molecular Model of
574 Kerogen's Nanostructure. *Nat. Mater.* **2016**, *15* (5), 576–582. <https://doi.org/10.1038/nmat4541>.
- 575 (71) Pei, Q.-X.; Zhang, Y.-W.; Shenoy, V. B. Mechanical Properties of Methyl Functionalized Graphene: A
576 Molecular Dynamics Study. *Nanotechnology* **2010**, *21* (11), 115709. <https://doi.org/10.1088/0957-4484/21/11/115709>.
- 577
- 578 (72) Lee, S. S.; Heberling, F.; Sturchio, N. C.; Eng, P. J.; Fenter, P. Surface Charge of the Calcite (104)
579 Terrace Measured by Rb⁺ Adsorption in Aqueous Solutions Using Resonant Anomalous X-Ray
580 Reflectivity. *J. Phys. Chem. C* **2016**, *120* (28), 15216–15223.
581 <https://doi.org/10.1021/acs.jpcc.6b04364>.
- 582 (73) Wolthers, M.; Tommaso, D. D.; Du, Z.; Leeuw, N. H. de. Calcite Surface Structure and Reactivity:
583 Molecular Dynamics Simulations and Macroscopic Surface Modelling of the Calcite–Water
584 Interface. *Phys. Chem. Chem. Phys.* **2012**, *14* (43), 15145–15157.
585 <https://doi.org/10.1039/C2CP42290E>.
- 586 (74) Berendsen, H. J. C.; van der Spoel, D.; van Drunen, R. GROMACS: A Message-Passing Parallel
587 Molecular Dynamics Implementation. *Comput. Phys. Commun.* **1995**, *91* (1), 43–56.
588 [https://doi.org/10.1016/0010-4655\(95\)00042-E](https://doi.org/10.1016/0010-4655(95)00042-E).
- 589 (75) Robertson, M. J.; Tirado-Rives, J.; Jorgensen, W. L. Improved Peptide and Protein Torsional
590 Energetics with the OPLS-AA Force Field. *J. Chem. Theory Comput.* **2015**, *11* (7), 3499–3509.
591 <https://doi.org/10.1021/acs.jctc.5b00356>.
- 592 (76) Berendsen, H. J. C.; Postma, J. P. M.; van Gunsteren, W. F.; Hermans, J. Interaction Models for
593 Water in Relation to Protein Hydration. In *Intermolecular Forces: Proceedings of the Fourteenth*
594 *Jerusalem Symposium on Quantum Chemistry and Biochemistry Held in Jerusalem, Israel, April 13–*
595 *16, 1981*; Pullman, B., Ed.; The Jerusalem Symposia on Quantum Chemistry and Biochemistry;
596 Springer Netherlands: Dordrecht, 1981; pp 331–342. https://doi.org/10.1007/978-94-015-7658-1_21.
- 597
- 598 (77) Raiteri, P.; Gale, J. D.; Quigley, D.; Rodger, P. M. Derivation of an Accurate Force-Field for
599 Simulating the Growth of Calcium Carbonate from Aqueous Solution: A New Model for the
600 Calcite–Water Interface. *J. Phys. Chem. C* **2010**, *114* (13), 5997–6010.
601 <https://doi.org/10.1021/jp910977a>.
- 602 (78) Geissbühler, P.; Fenter, P.; DiMasi, E.; Srajer, G.; Sorensen, L. B.; Sturchio, N. C. Three-Dimensional
603 Structure of the Calcite–Water Interface by Surface X-Ray Scattering. *Surf. Sci.* **2004**, *573* (2), 191–
604 203. <https://doi.org/10.1016/j.susc.2004.09.036>.
- 605 (79) Wolf, G.; Lerchner, J.; Schmidt, H.; Gamsjäger, H.; Königsberger, E.; Schmidt, P. Thermodynamics of
606 CaCO₃ Phase Transitions. *J. Therm. Anal. Calorim.* **1996**, *46* (2), 353–359.
607 <https://doi.org/10.1007/BF02135013>.
- 608 (80) Wolf, G.; Königsberger, E.; Schmidt, H. G.; Königsberger, L.-C.; Gamsjäger, H. Thermodynamic
609 Aspects of the Vaterite–Calcite Phase Transition. *J. Therm. Anal. Calorim.* **2000**, *60* (2), 463–472.
610 <https://doi.org/10.1023/A:1010114131577>.
- 611 (81) Humphrey, W.; Dalke, A.; Schulten, K. VMD: Visual Molecular Dynamics. *J. Mol. Graph.* **1996**, *14*
612 (1), 33–38. [https://doi.org/10.1016/0263-7855\(96\)00018-5](https://doi.org/10.1016/0263-7855(96)00018-5).
- 613 (82) Kumar, S.; Rosenberg, J. M.; Bouzida, D.; Swendsen, R. H.; Kollman, P. A. THE Weighted Histogram
614 Analysis Method for Free-Energy Calculations on Biomolecules. I. The Method. *J. Comput. Chem.*
615 **1992**, *13* (8), 1011–1021. <https://doi.org/10.1002/jcc.540130812>.
- 616 (83) Roux, B. The Calculation of the Potential of Mean Force Using Computer Simulations. *Comput.*
617 *Phys. Commun.* **1995**, *91* (1), 275–282. [https://doi.org/10.1016/0010-4655\(95\)00053-I](https://doi.org/10.1016/0010-4655(95)00053-I).

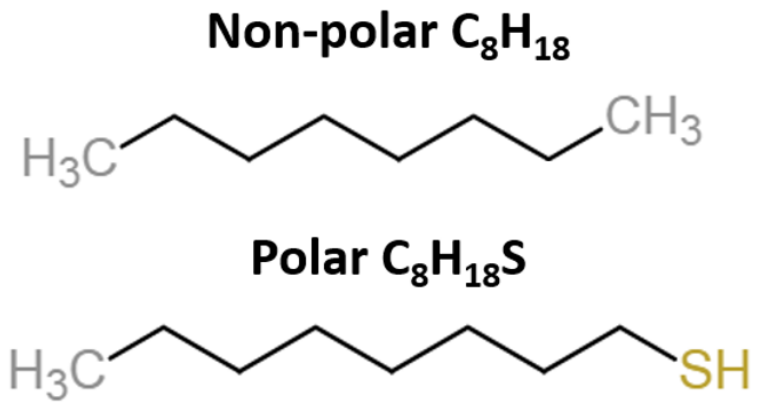
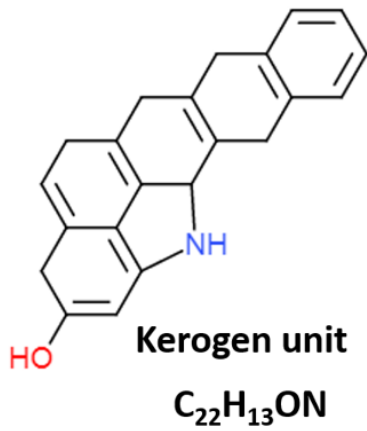
- 618 (84) Hub, J. S.; de Groot, B. L.; van der Spoel, D. G. gwham—A Free Weighted Histogram Analysis
619 Implementation Including Robust Error and Autocorrelation Estimates. *J. Chem. Theory Comput.*
620 **2010**, *6* (12), 3713–3720. <https://doi.org/10.1021/ct100494z>.
- 621 (85) Cleveland, W. S. Robust Locally Weighted Regression and Smoothing Scatterplots. *J. Am. Stat.*
622 *Assoc.* **1979**, *74* (368), 829–836. <https://doi.org/10.1080/01621459.1979.10481038>.
- 623 (86) R Core Team. *R: A Language and Environment for Statistical Computing*; R Foundation for
624 Statistical Computing: Vienna, Austria, 2019.
- 625 (87) Hakim, S. S.; Olsson, M. H. M.; Sørensen, H. O.; Bovet, N.; Bohr, J.; Feidenhans'l, R.; Stipp, S. L. S.
626 Interactions of the Calcite {10.4} Surface with Organic Compounds: Structure and Behaviour at
627 Mineral – Organic Interfaces. *Sci. Rep.* **2017**, *7* (1), 7592. [https://doi.org/10.1038/s41598-017-](https://doi.org/10.1038/s41598-017-06977-4)
628 [06977-4](https://doi.org/10.1038/s41598-017-06977-4).
- 629 (88) Ross, D. J. K.; Bustin, R. M. Shale Gas Potential of the Lower Jurassic Gordondale Member,
630 Northeastern British Columbia, Canada. *Bull. Can. Pet. Geol.* **2007**, *55* (1), 51–75.
631 <https://doi.org/10.2113/gscpgbull.55.1.51>.
- 632 (89) Loucks, R. G.; Reed, R. M.; Ruppel, S. C.; Jarvie, D. M. Morphology, Genesis, and Distribution of
633 Nanometer-Scale Pores in Siliceous Mudstones of the Mississippian Barnett Shale. *J. Sediment. Res.*
634 **2009**, *79* (12), 848–861. <https://doi.org/10.2110/jsr.2009.092>.
- 635 (90) Madsen, L.; Grahl-Madsen, L.; Grøn, C.; Lind, I.; Engell, J. Adsorption of Polar Aromatic
636 Hydrocarbons on Synthetic Calcite. *Org. Geochem.* **1996**, *24* (12), 1151–1155.
637 [https://doi.org/10.1016/S0146-6380\(96\)00096-4](https://doi.org/10.1016/S0146-6380(96)00096-4).
- 638 (91) García Carmona, J.; Gómez Morales, J.; Rodríguez Clemente, R. Rhombohedral–Scalenohedral
639 Calcite Transition Produced by Adjusting the Solution Electrical Conductivity in the System
640 Ca(OH)₂–CO₂–H₂O. *J. Colloid Interface Sci.* **2003**, *261* (2), 434–440.
641 [https://doi.org/10.1016/S0021-9797\(03\)00149-8](https://doi.org/10.1016/S0021-9797(03)00149-8).
- 642 (92) Shen, J.-W.; Li, C.; van der Vegt, N. F. A.; Peter, C. Understanding the Control of Mineralization by
643 Polyelectrolyte Additives: Simulation of Preferential Binding to Calcite Surfaces. *J. Phys. Chem. C*
644 **2013**, *117* (13), 6904–6913. <https://doi.org/10.1021/jp402341w>.
- 645



646

647

Figure 1. Effect of intermolecular interaction on the fluid confined in nanostructures.



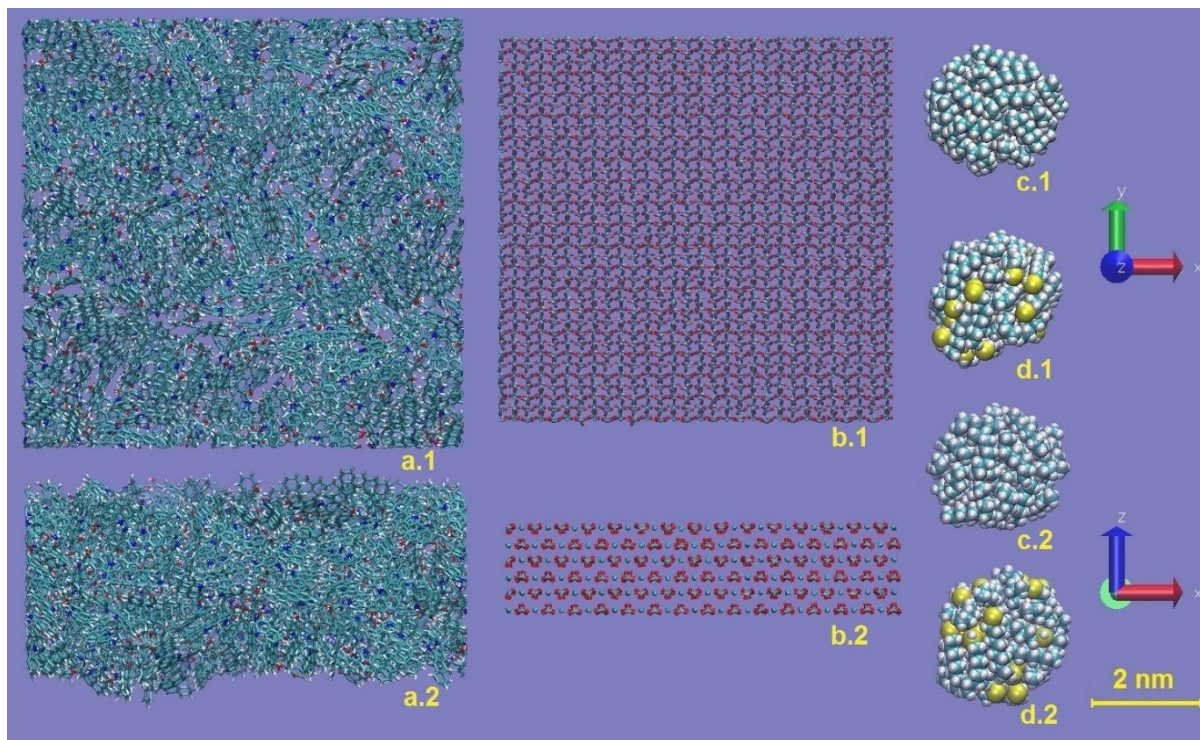
648

649

650

651

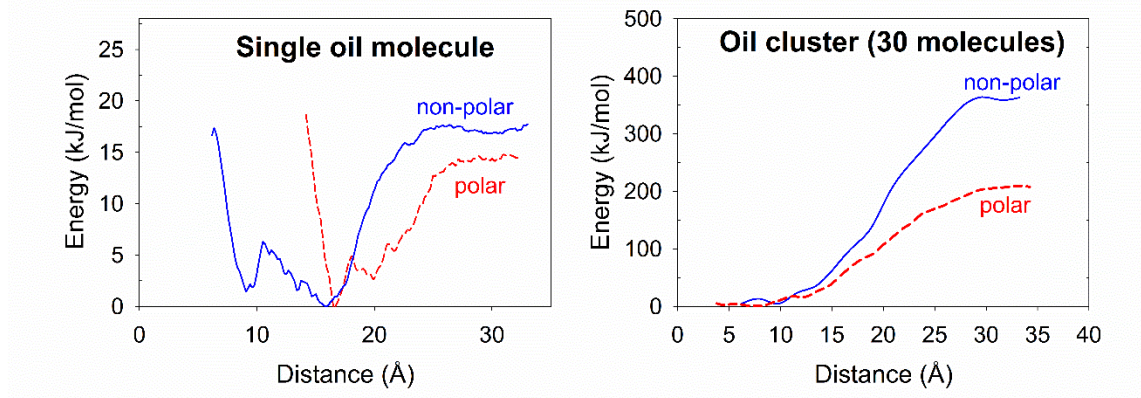
Figure 2. Molecular structure of type II kerogen fragment (left), non-polar oil n-octane (right top), and polar oil 1-octanethiol (right bottom).



652

653 Figure 3. Kerogen slab (a), calcite (104) slab (b), 30-molecule non-polar oil cluster (c), and 30-molecule
 654 polar oil cluster (d). “x.1” and “x.2” denote different orientations.

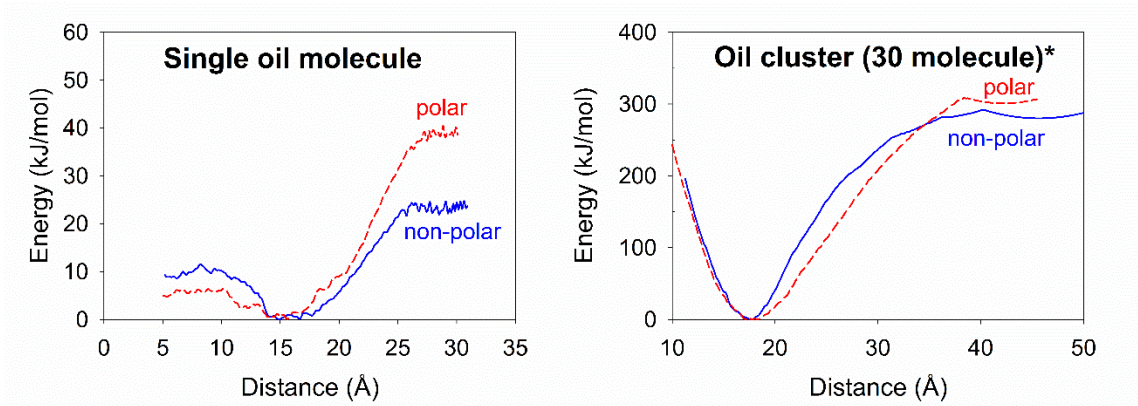
655



656

657 Figure 4. Free energy surfaces of single molecule of polar or non-polar oil on kerogen surface with water
 658 (left); Free energy surfaces of oil drop of 30 polar or non-polar oil molecules on kerogen surface with
 659 water (right).

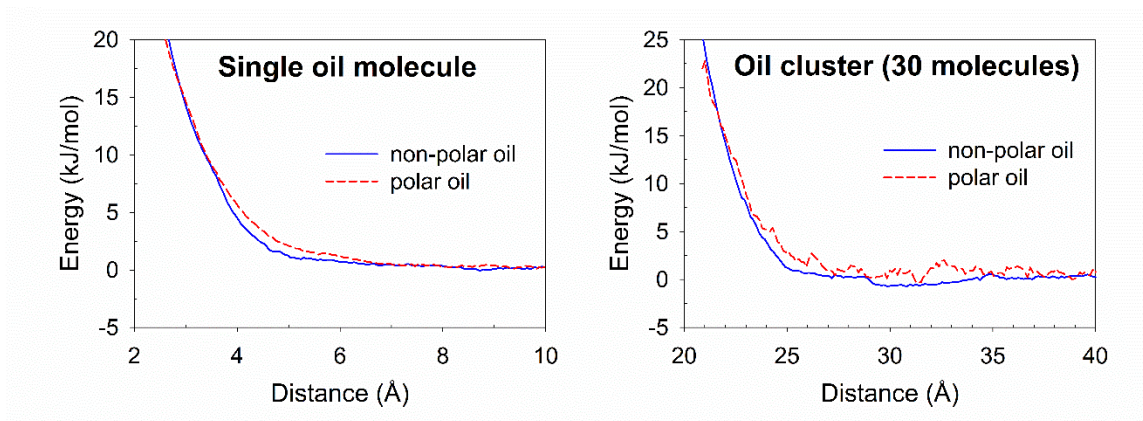
660



661

662 Figure 5. Free energy surfaces of single molecule of polar and non-polar oil on kerogen surface without
 663 water (left); free energy surfaces of oil drop of 30 polar or non-polar oil molecules on kerogen surface
 664 without water (right). *indicates the simulations were prepared at 200K due to the technical issues as
 665 described in the discussion.

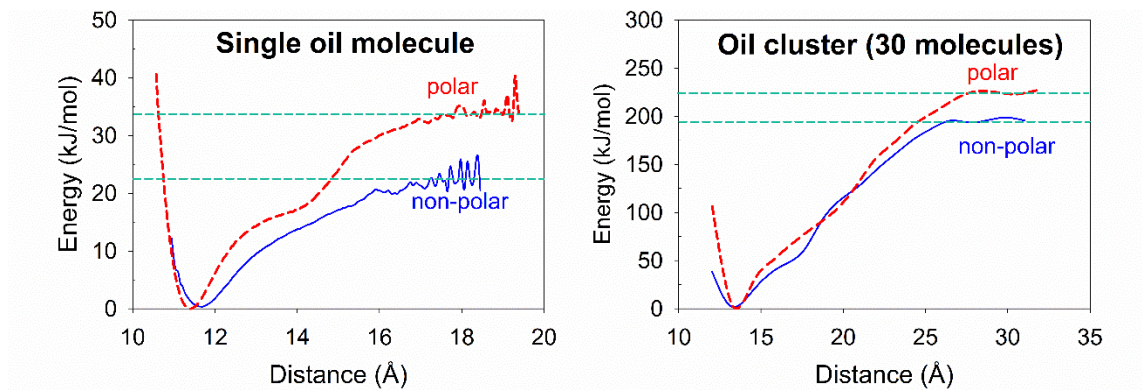
666



667

668 Figure 6. Free energy surfaces of single molecule and 30-molecule cluster of polar or non-polar oil on
 669 calcite surface in the presence of water.

670



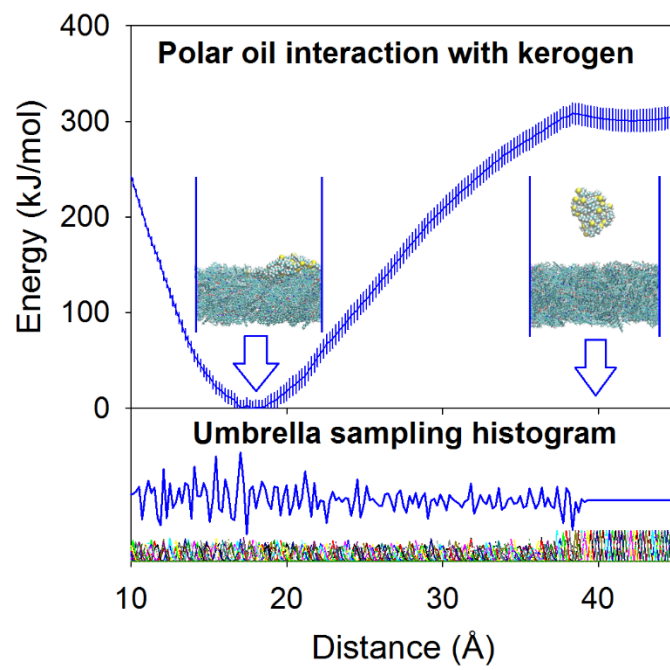
671

672 Figure 7. Free energy surfaces of single molecule of polar or non-polar oil on calcite surface without
 673 water (left); free energy surfaces of oil drop of polar or non-polar oil on calcite surface without water
 674 (right).

675

Table 1. Desorption energy of single molecule oil droplet and 30-molecule oil drop on calcite and kerogen surface under 300 K. The () denotes the errors propagated from the output data of WHAM.

Desorption energy (kJ/mol)		Kerogen with water	Kerogen	Calcite with water	Calcite
Non-polar oil	Single molecule	17.0 (2.0)	23.3 (3.5)	0	18.0 (5.5)
	Cluster - total	372 (13.8)	438 (13.5)	0	198 (42)
	Cluster - per molecule	12.4 (0.46)	14.6 (0.45)	0	6.6 (1.4)
Polar oil	Single molecule	16.5 (3.3)	39.5 (9.5)	0	33.6 (3.9)
	Cluster - total	210 (11.4)	438 (13.5)	0	222 (36)
	Cluster - per molecule	7.0 (0.38)	14.6 (0.45)	0	7.4 (1.2)



Supporting Information

Energetics of Interfacial Interactions of Hydrocarbon Fluids with Kerogen and Calcite using Molecular Modeling

Zelong Zhang,^{*,†} Haoran Liu,^{‡,⊥} and Jianwei Wang^{†,§}

[†]Department of Geology and Geophysics, Louisiana State University, Baton Rouge, LA 70803, United States

[‡]Department of Experimental Statistics, Louisiana State University, Baton Rouge, LA 70803, United States

[⊥]Department of Oceanography and Coastal Sciences, Louisiana State University, Baton Rouge, LA 70803, United States

[§]Center for Computation and Technology, Louisiana State University, Baton Rouge, LA 70803, United States

Corresponding to: zelongz@lsu.edu

Table of Contents

Supporting text 1: Code for error estimation performed by RStudio.

Supporting text 2: Video links of pertinent simulation trajectories.

Figure S1: Free energy surfaces of a single molecule and cluster of 30 polar or non-polar oil molecules on calcite (104) in the presence of water.

Figure S2: Free energy surfaces of cluster of 30-molecule polar and non-polar oil molecules on kerogen surface under different temperatures.

Figure S3: Desorption energies of 30-molecule oil clusters on kerogen surfaces under different temperatures.

Figure S4: Snapshot of the simulation trajectory of calcite surface interaction with a polar oil molecule in the absence of water.

Figure S5: Snapshot of the simulation trajectory of kerogen surface interaction with a polar oil molecule in the absence of water at different time step.

Table S1: Desorption energies of 30-molecule oil clusters on kerogen surfaces under different temperatures in the absence of water.

Supporting Information

Code for error estimation performed by RStudio

```
library(bootstrap)
attach(dat)

B<-150
boot.fit<-matrix(0,B,length(x))

for (i in 1:B){
  set.seed(i)
  indx <- sample(1:178,size=178,replace=T)

  fit <- loess(y~x,dat[indx,],span=0.30)

  boot.fit[i,] <- predict(fit,x)
}

FUN<-function(x){
  quantile(x,prob=c(.025,.975),na.rm=T) # calculate 95% CI
}
boot.CI<-apply(boot.fit,2,FUN)

y_2.5<-boot.CI[1,]
y_97.5<-boot.CI[2,]
```

Supporting Information

Video links of pertinent simulation trajectories

100 ps MD trajectory of a polar oil molecule interaction with kerogen surface

<https://youtu.be/ITlvF7TlyMg>

100 ps MD trajectory of a polar oil molecule interaction with frozen kerogen surface

<https://youtu.be/P2AXQOT4W1E>

1 ns MD trajectory of a polar oil molecule interaction with frozen kerogen surface

<https://youtu.be/iL8cv0Mprcg>

100 ps MD trajectory of a non-polar oil molecule interaction with kerogen surface

<https://youtu.be/zmdeLdsBWsq>

100 ps MD trajectory of a polar oil molecule interaction with calcite (104) surface

<https://youtu.be/crq9xLuhik>

100 ps MD trajectory of a non-polar oil molecule interaction with calcite (104) surface

<https://youtu.be/B0WEq0kv7yA>

Supporting Information

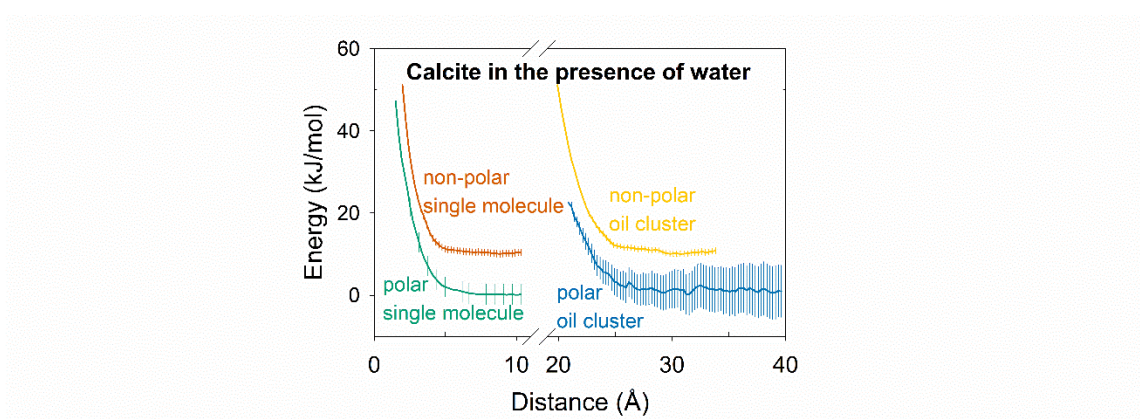


Figure S1. Free energy surfaces of a single molecule and cluster of 30 polar or non-polar oil molecules on calcite (104) in the presence of water. The free energy surfaces are plotted as a function of distance between the oil molecule / oil cluster and calcite surface with respect to their centers of mass. The density of displayed data is reduced for visual clarity.

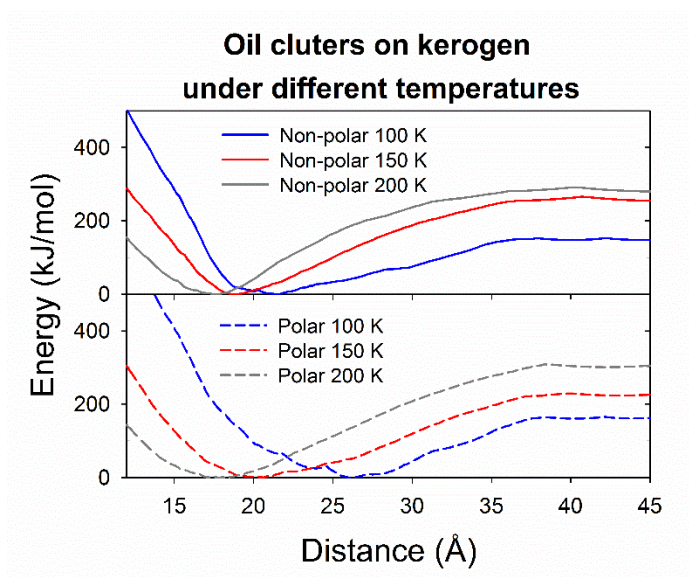


Figure S2. Free energy surfaces of cluster of 30-molecule polar and non-polar oil molecules on kerogen surface under different temperatures. The free energy surfaces are plotted as a function of distance between the oil cluster and kerogen surface with respect to their centers of mass. According to the data point pattern, the correlation between desorption energy and temperature can be formulated using the same linear equation as shown in Figure S3 for both polar and non-polar oil. The error bars are smaller than the symbol size.

Supporting Information

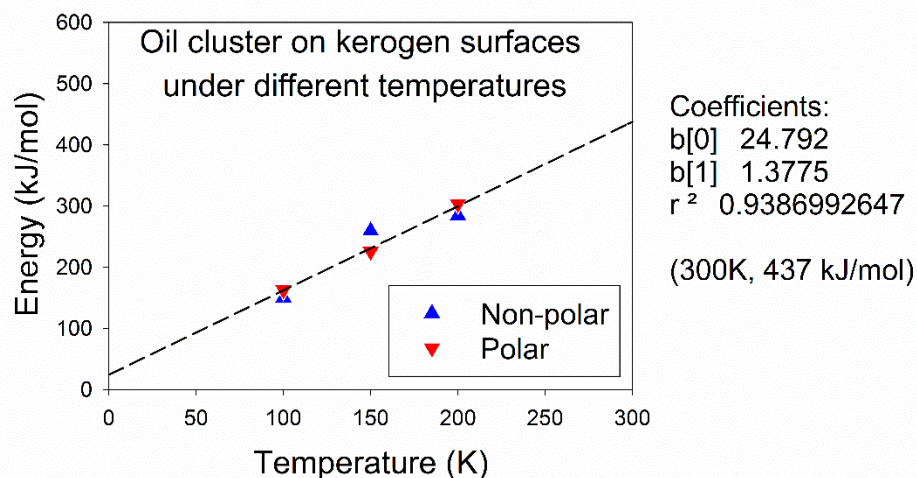


Figure S3. Desorption energies of 30-molecule oil clusters on kerogen surfaces under different temperatures. The non-polar and polar oil drops exhibit linear relationship between temperature and desorption energy (with a R-squared value of 0.9387). The non-polar and polar oil drops follow the same correlation between desorption energy (E_d in kJ/mol) and temperature (T in K):

$$E_d = 1.38 \cdot T + 24.8$$

The energy required for oil drop desorption from kerogen surface increases when the system temperature rises. As shown in Figure S5, a close examination on the interface of oil and surface reveals that oil molecule is strongly attached to the kerogen surface. The same correlation of energy and temperature suggested that the intermolecular bonding between kerogen and oil are so strong that the effect of oil polarity is negligible in such interactions.

Supporting Information

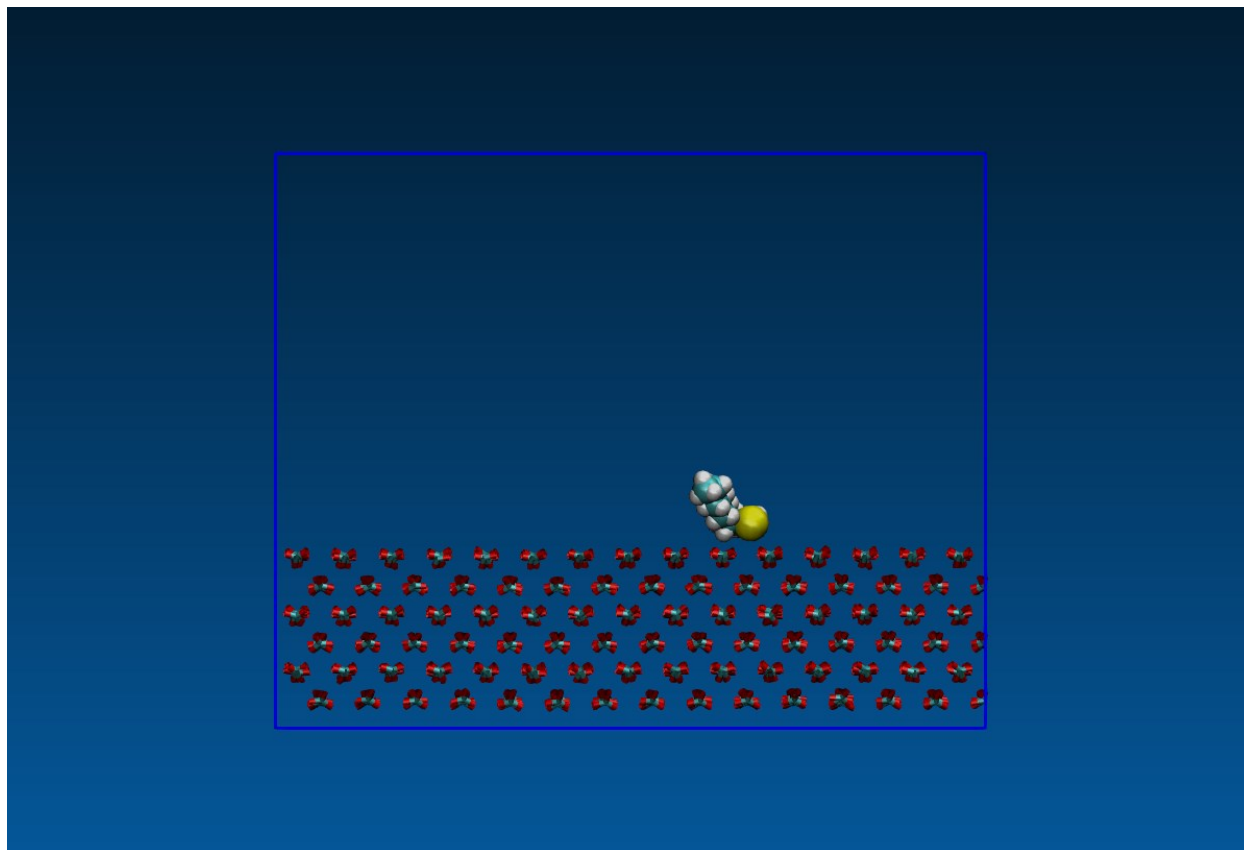


Figure S4. Snapshot of the simulation trajectory of calcite surface interaction with a polar oil molecule in the absence of water.

Supporting Information

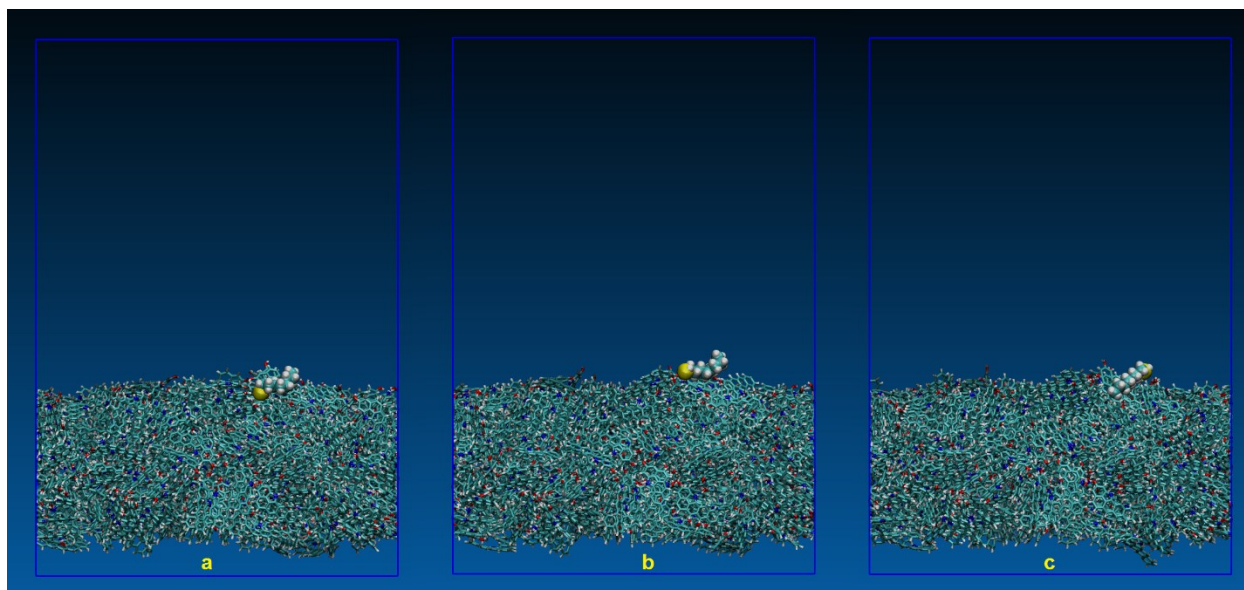


Figure S5. Snapshot of the simulation trajectory of kerogen surface interaction with a polar oil molecule in the absence of water at different time step. (a) and (b) depict strong interactions between polar oil functional group $-SH$ and kerogen functional groups $-NH-$ and $-OH$, whereas (c) illustrates strong interactions between non-polar carbon chain of polar oil and non-polar benzene rings of kerogen.

Supporting Information

Table S1. Desorption energies of 30-molecule oil clusters on kerogen surfaces under different temperatures in the absence of water.

Desorption energy in kJ/mol [error]		
Temperature	Non-polar	Polar
100 K	150.5 [2.5]	163 [3]
150 K	260 [5.5]	226 [3]
200 K	285 [5.5]	304 [5]